Journal Name

ARTICLE TYPE

Cite this: DOI: 10.1039/xxxxxxxxxx

Flow-driven Control of Calcium Carbonate Precipitation Patterns in a Confined Geometry†

Gábor Schuszter, Fabian Brau, and A. De Wit*

Received Date
Accepted Date

DOI: 10.1039/xxxxxxxxxx

www.rsc.org/journalname

Upon injection of an aqueous solution of carbonate into a solution of calcium ions in the confined geometry of a Hele-Shaw cell, various calcium carbonate precipitation patterns are observed. We discuss here the properties of these precipitation structures as a function of the injection flow rate and concentrations of the reactants. We show that such flow-controlled conditions can be used to influence the total amount and the spatial distribution of the solid phase produced as well as the reaction efficiency defined here as the amount of product formed for a given initial concentration of the injected solution.

1 Introduction

Depending on the operating conditions, a precipitation reaction can generate a solid product in variable amount, spatial distribution, and physico-chemical properties. A simple way to experimentally perform precipitation consists in pouring all reactants in a well-stirred reactor where the stirring ensures a fast mixing yielding ultimately a relatively homogeneous suspension of equilibrium precipitate product. Precipitation can also occur in a gel or solid matrix through diffusion of reactants as seen in biomineralization[1,2], Liesegang rings in sedimentary rocks[3] or in counterdiffusion crystallisation methods used to produce macromolecular protein crystals for instance[4]. However, this precipitation procedure is slow and produces precipitates embedded in a gel or solid matrix making their separation problematic if the product needs to be collected.

Flow-driven precipitation, where one reactant solution is injected into the other one is another promising technique producing precipitates in non-equilibrium conditions[5–7]. Such a technique is nowadays attracting increased attention because gradients induced by the flow or hydrodynamic instabilities may lead to new synthesis modes. For example, it has recently been shown that flow-driven precipitation can affect crystallization kinetics[8], lead to the enrichment, compared to well-stirred conditions, of thermodynamically unstable polymorphs[9,10], spatial segregation of different crystalline structures along the spreading direction[6,11], directionally asymmetric self-assembly[12,13], or can be used to control the microstructure of the precipitate[14].

At the macroscopic level, the presence of flows can influence the precipitation patterns obtained and produce a wide variety of complex forms[7,12,15–18]. As an example, chemical gardens growing in 3D when placing solid metal salt seeds into alkaline solutions such as silicate are shaped by buoyancy-driven flows among other processes[19]. Control of the growth dynamics of these 3D structures has been attempted succesfully using bubble driving[20], microgravity conditions[21], microfluidics[22], or injection of one reactant into the other[5]. In confined quasi 2D geometries, such a flow-control has allowed to obtain in a reproductive way a wealth of different patterns when the concentration of the various chemicals are varied[7,12,16,17]. Hydrodynamic instabilities can shape some of the structures at lower concentrations: as an example, needles of precipitate may align along convective rolls induced by a buoyancy instability[11,23], a viscous fingering instability can shape the precipitate into flowers[17] or local changes in permeability can trigger fingered patterns[15,18,24]. At larger concentrations, mechanical effects due to the cohesion of the solid phase can select other forms like spirals[7] or filaments[7,12,16] that are robust with changes in the reactants[16]. These examples highlight the importance of concentration gradients and convective mixing induced by flow conditions for the production of new materials as well as controlling the micro structure of the solid and/or its macroscopic self-organization.

In this context, our objective is to discuss the influence of flow conditions on optimizing various quantities characterizing the amount and spatial distribution of a solid phase produced when an aqueous solution of one reactant of a precipitation reaction is injected in a solution of the other reactant. To do so, we analyze experimentally macroscopic calcium carbonate patterns produced by injecting radially in a confined geometry an aqueous solution of carbonates (CO_3^{2-}) into a solution of calcium

Université libre de Bruxelles (ULB), Nonlinear Physical Chemistry Unit, CP231, 1050 Brussels, Belgium. Fax: +32 2 650 5767; Tel: +32 2 650 5774;
E-mail: adewit@ulb.ac.be

† Electronic Supplementary Information (ESI) available: [Description of solution properties (S1); Ion activity product and solubility product (S2); Detailed image analysis (S3)]. See DOI: 10.1039/b000000x/

* To whom correspondence should be addressed

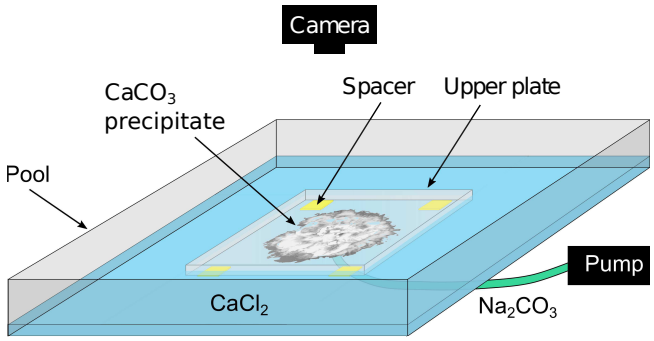

Fig. 1 The thin reaction area is confined by two Plexiglas plates (the upper plate and the pool) and filled with Ca^{2+} solution while a CO_3^{2-} solution is injected by a syringe pump through a tiny inlet from below.

ions (Ca^{2+}). White $CaCO_3$ precipitate appears along the moving miscible interface between the two reactants according to a precipitation reaction $Ca^{2+} + CO_3^{2-} \rightarrow CaCO_3(s)$ typically important for mineralisation of CO_2 in soil sequestration processes[18,25–29]. We have recently shown that coupling between this precipitation reaction and injection can lead to a drastic drop of the amount of precipitate even if the reactant concentrations are large in the vicinity of the reaction zone[18]. In order to better understand how the quantity of calcium carbonate and its spatial distribution depend on reactant concentrations and flow rate, the temporal and spatial evolution of the precipitate patterns are analyzed. Various quantities such as the total gray scale intensity of the pattern, its filling, density or brightness are monitored as a function of time. We also compute the precipitation efficiency defined here as the amount of the solid phase produced per concentration of the injected reactant.

We show that finding optimal precipitation conditions such that all these quantities are maximized is a challenge, even in a simple Hele-Shaw setup like the one used here.

2 Materials and Methods

Experiments are carried out in a horizontal confined geometry maintained between a large lower pool (35 cm $\times$ 35 cm) and a smaller upper plate (21 cm $\times$ 21 cm) made of transparent Plexiglas (Fig. 1) vertically separated by a small interstice (0.5 mm) thanks to 4 spacers. The setup is illuminated from above by two light pads placed symmetrically with respect to a digital camera recording the dynamics (PixeLINK B742U giving images of $N = 1280 \times 1024$ pixels).

The gap of the cell is initially filled by an aqueous solution of calcium chloride $CaCl_2$. The same solution is then poured around the upper plate, into the pool, to form a 4 mm thick liquid layer. This outer layer is in contact with the 0.5 mm thin layer within the gap and ensures a spatially homogeneous outflow along the sides of the upper plate during the experiment. An aqueous solution of sodium carbonate Na_2CO_3 is next injected radially from the center of the lower pool through an inlet of 1 mm inner diameter using a syringe pump (kdScientific 210P-CE). A fixed total volume of 2.5 mL of solution is injected in all experiments at a given constant flow rate $Q = 0.1$, 1.0, and 6.5 mL/min. The experiments are performed for variable initial concentrations of reactants at $T = (21 \pm 1)^\circ$C. The properties of the reactant solutions are given in Supporting Information S1. The initial pH of the carbonate solution is maintained to 10 by addition of HCl to avoid the formation of $Ca(OH)_2$ precipitate. During the experiments, the white $CaCO_3$ precipitate is produced by the reaction $Ca^{2+}_{(aq)} + CO^{2-}_{3\,(aq)} \rightleftharpoons CaCO_{3(s)}$. For each set of experimental values tested, the experiment is reproduced three times. Examples of the three patterns obtained for the same values of parameters and same initial conditions are presented in the Supporting Information S2. The reproducibility of the pattern is very good and hence the type of structures obtained for a given value of parameters is robust.

3 Precipitation Patterns

Upon injection of one reactant solution into the other one, a white $CaCO_3$ precipitate layer is formed and various shapes can be observed as shown in Fig. 2 displaying the precipitation patterns as a function of initial reactant concentrations and injection flow rate[18].

At given initial concentrations of reactants, the tendency of the system to form a precipitate may be characterized by the saturation index $SI_0 = \log_{10}(IAP_0/K_{SP})$ where IAP_0 and K_{SP} are the initial ion activity product of the reactant solutions and the solubility product of $CaCO_3$ respectively (see Supporting Information S3 for detailed description). SI_0 varies thus with the reactant concentrations and the larger SI_0, the larger the thermodynamic force to form a precipitate. In our experiments, the system is largely supersaturated for all concentrations scanned ($SI_0 > 1$ in all panels of Fig. 2) and precipitation is expected in all cases. Counterintuitively, we see that the smallest amount of precipitate is obtained at the largest concentrations (highest SI_0) and flow rate (see Fig. 2b5,c5)

The influence of the flow rate is shown in Fig. 2 by analyzing the patterns along a column for which the initial reactant concentrations, and thus SI_0, are constant while Q increases downwards. We see that at low flow rate and below some threshold for both concentrations, the patterns remain mainly circular during their growth with a rather homogeneous distribution of precipitate (Fig. 2a1-4). This homogeneity and symmetry is broken when the flow increases because the precipitate is then advected away from the inlet region and accumulates at the periphery, near the miscible reactive interface (Fig. 2b1-3). The permeability in this region is then significantly reduced which leads to the emergence of a fingering instability deforming the pattern periphery at larger concentrations and flow rate (Fig. 2b4 and c1-4)[15]. Note that here $M = \mu_{0,Ca^{2+}}/\mu_{0,CO_3^{2-}} > 1$, where M is the ratio between the initial viscosity of the displaced solution $\mu_{0,Ca^{2+}}$ and that of the injected solution $\mu_{0,CO_3^{2-}}$. $M > 1$ refers to a viscously unstable situation leading to the emergence of a fingering instability. However, as shown previously[17], for the flow rates used here and on the timescale of the experiments, M is not large enough to lead to viscous fingering in the non-reactive case. The mechanism of fingering results thus rather from the local decrease of permeability.

Surprisingly, the patterns obtained at medium and large Q with the largest SI_0 are those characterized by the smallest amount of precipitate (Fig. 2b5,c5). These examples highlight the strong

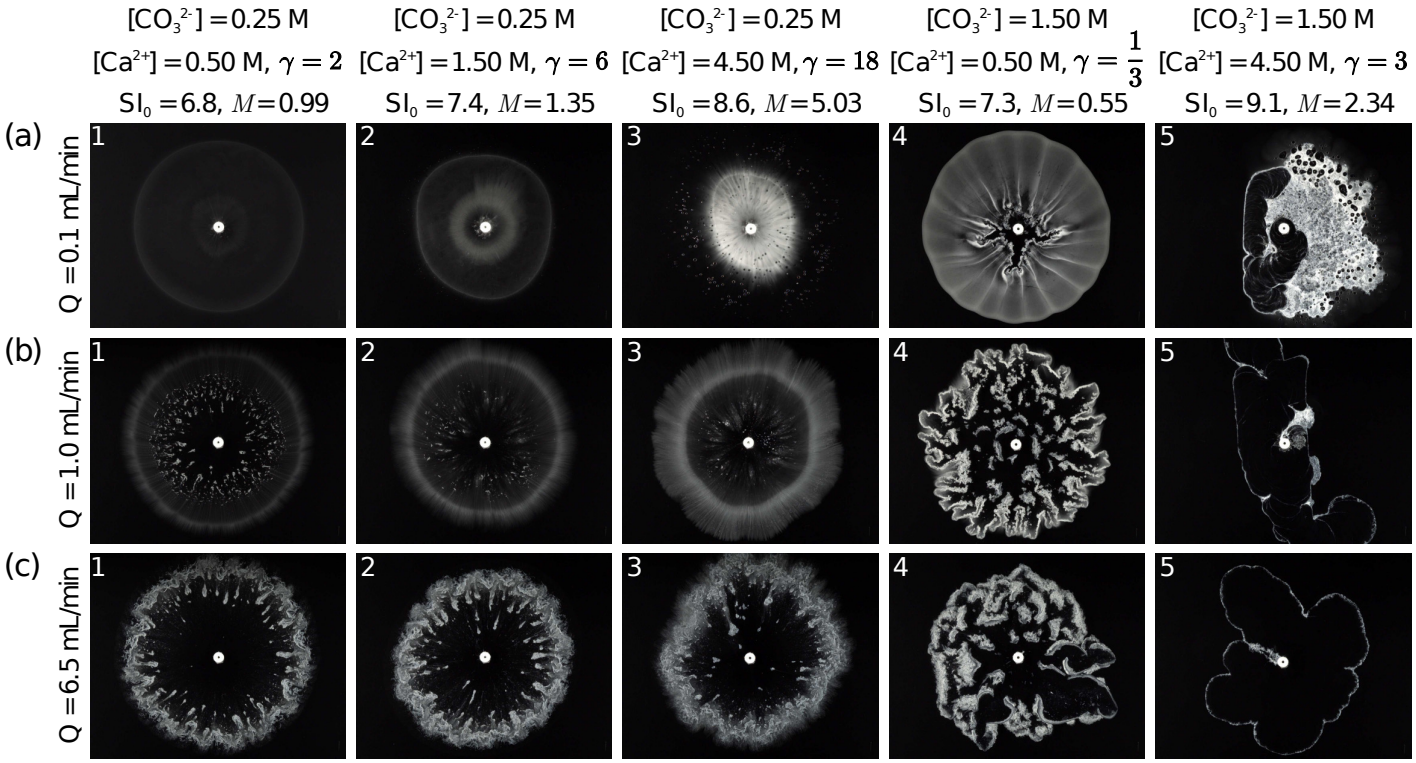

Fig. 2 Precipitate patterns observed at different flow rates and concentrations after injecting 2.5 mL of carbonate solution. Field of view: 123 mm × 98 mm. The number in the top left corner of the images is the number of the pattern. In the header, the stoichiometric ratio of the reactants $\gamma = [Ca^{2+}]_0/[CO_3^{2-}]_0$, the saturation index $SI_0 = \log_{10}(IAP_0/K_{SP})$ where IAP_0 and K_{SP} are the initial ion activity product of the reactant solutions and the solubility product of $CaCO_3$, and the viscosity contrast of the reactant solutions $M = \mu_{0,Ca^{2+}}/\mu_{0,CO_3^{2-}}$ are presented.

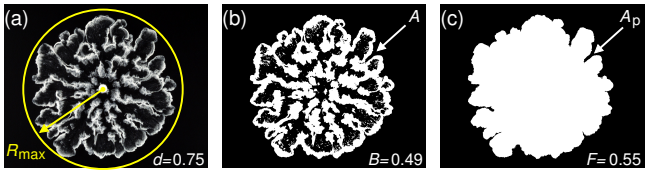

Fig. 3 Quantities used to characterize the patterns. (a) gray scale intensity $I(x,y)$ used to compute I_{tot} and d. The yellow circle centered on the inlet and passing by the tip of the longest finger defines the radius R_{max}. (b) The area A of the region covered by the solid phase is used to compute $B = I_{tot}/A$. (c) The area A_p inside the pattern perimeter is used to compute $F = A/A_p$.

effects of the coupling between chemical reactions and hydrodynamics on precipitation in a confined geometry. Let us analyze how this coupling can control the precipitate properties produced in confined geometry in flow conditions.

4 Pattern Characterization

A large variety of precipitation patterns is thus observed when reactant concentrations and flow rates are varied (Fig. 2). To study those patterns, we first define the ratio of the initial reactant concentrations as $\gamma = [Ca^{2+}]_0/[CO_3^{2-}]_0$, where $[Ca^{2+}]_0$ and $[CO_3^{2-}]_0$ are the initial concentrations of the calcium and carbonate solutions, respectively. $\gamma > 1$ means that the displaced solution is in stoichiometric excess compared to the injected one.

A quantitative image analysis is performed on the basis of seven quantities: (*i*) The area A covered by the precipitate (Fig. 3b); (*ii*) The area A_p enclosed by the pattern perimeter (Fig. 3c); (*iii*) The total gray scale intensity $I_{tot} \in [0,A]$ of the white precipitate in a given image; (*iv*) The brightness $B = I_{tot}/A \in [0,1]$ measuring the compactness of the precipitate; (*v*) The filling $F = A/A_p \in [0,1]$ measuring how the pattern is filled by the precipitate; (*vi*) the pattern density $d = A_p/(\pi R_{max}^2) \in [0,1]$ measuring the deviation from a circular growth (Fig. 3a); and (*vii*) the production efficiency $P = I_{tot}/c_{0,CO_3^{2-}}$ measuring how much precipitate is produced for a given initial concentration of the injected reactant. More details about these quantities can be found in Ref.[18] and in the Supporting Information S4.

All those quantities are measured on the images of three independent experiments performed with the same parameter values in order to compute their averages and standard deviations. The errors bars are generally quite small showing that the measured quantities do not fluctuate significantly for given values of parameters.

5 Precipitation Efficiency

The quantities listed in Sec. 4 characterize our confined precipitation patterns from different view points. They may be used to analyze the efficiency of the precipitate production depending on which characteristic is considered. The different identified optimal regimes are listed in Table 1.

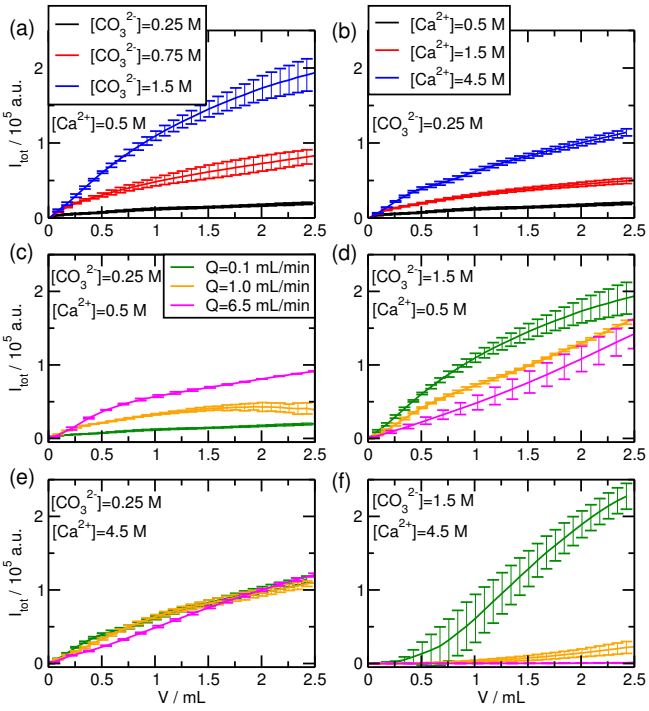

Fig. 4 Evolution of the total grayscale intensity I_{tot} as a function of injected volume V of carbonate solution. $Q = 0.1$ mL/min for (a–b).

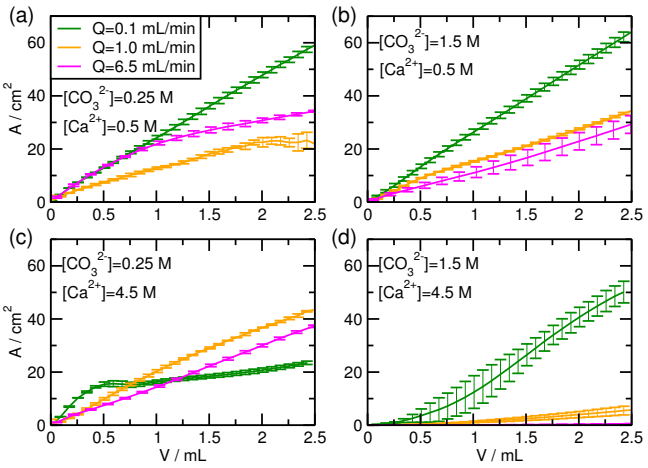

Fig. 5 Evolution of the area A covered by the pattern as a function of injected volume V of carbonate solution at different flow rates and initial reactant concentrations.

5.1 Amount of Precipitate

We first consider the efficiency of precipitation assuming that the production of the largest amount of precipitate is required. The evolution of I_{tot}, which is a semi-quantitative indicator of the amount of precipitate in the cell, is depicted in Fig. 4 as a function of the injected volume V for different experimental conditions. The same scale is used on all graphs to facilitate the comparison.

We see that, when the concentration of one of the reactants is low, I_{tot} increases with the concentration of the other reactant (Fig. 4a,b). Injecting CO_3^{2-} solution with a large concentration into a Ca^{2+} solution with low concentration (Fig. 4a) produces more precipitate than the opposite case (Fig. 4b) even if the values of their SI_0 predicts the reverse ($SI_0 = 7.3$ and $SI_0 = 8.6$, respectively, see Fig. 2). This shows that I_{tot} depends not only on SI_0 but also on the ratio γ of initial concentrations.

The effect of increasing the injection rate Q on I_{tot} is shown in Fig. 4c–f for different initial couples of concentrations. For low concentrations of both reactants, the amount of precipitate increases with Q which induces a better mixing between the solutions (Fig. 4c and first column of Fig. 2). One could therefore expect that the largest amount of precipitate is produced when both solutions are concentrated and Q is large. As shown in Fig. 4f, this is not the case: when the concentrations of both reactants are large, the largest I_{tot} is reached at low flow rate, while the amount of precipitate sharply drops if Q is increased (Fig. 4f and Fig. 2b5,c5). The large value of SI_0 together with the moderate stoichiometric excess of the displaced solution ($\gamma = 3$) lead in that case to the production of a large amount of precipitate in small localized regions forming solid walls hindering further mixing. The subsequent production of precipitate sharply drops. Therefore, a reaction producing a large amount of cohesive precipitate over a small length scale has a negative feedback at a much larger scale.

In conclusion, the largest amount of precipitate is produced at low flow rate when the concentration of the injected CO_3^{2-} solution is large.

5.2 Spatial Distribution of Patterns

In some applications like CO_2 mineralization in soils, a target might be to obtain a homogeneous distribution of precipitate on the widest possible area. However, the patterns are not always fully homogeneous. To study the spatial distribution of the precipitate and its deviation from an ideal homogeneous radial structure, we consider the evolution of two quantities, the filling F and the pattern density d as a function of the volume of the injected CO_3^{2-} solution. To do so, we discuss first the area A covered by the precipitate and the area A_p enclosed by its perimeter.

5.2.1 Area A Covered by the Precipitate.

The evolution as a function of the injected volume V of the area A covered by the precipitate is shown in Fig. 5. When both reactants have low concentrations (Fig. 5a), the lowest flow rate gives the largest A because the precipitate is spread more or less homogeneously within the pattern perimeter (Fig. 2a1). Increasing Q lowers the area A because the precipitate is then flushed away from the inlet region and accumulates at the pattern periphery (Fig. 2c1). However, this decrease of A with increasing Q is not monotonic, because a larger amount of precipitate is also produced at larger Q for these reactant concentrations (Fig. 4c and Fig. 5a).

A similar trend is observed when a concentrated solution of CO_3^{2-} is injected into a less concentrated solution of Ca^{2+} (Fig. 5b). Again, the largest value of A is obtained at low flow rates and increasing Q lowers A. Indeed, for low injection rate, the precipitate is distributed almost homogeneously (Fig. 2a4), whereas, for larger Q, fingering appears inducing an accumulation of precipitate at the rim of the fingers (Fig. 2b4,c4). Even if γ and SI_0 remain constant, injection at a faster rate leads to the

production of more precipitate per given area which increases the unfavorable mobility gradient between the precipitate layer and the injected fluid. In contrast, the absolute amount of precipitate does not significantly vary with Q (Fig. 4d) leading to a decrease of A.

In the opposite case, *i.e.* when the displaced solution of Ca^{2+} is in large stoichiometric excess (Fig. 5c), the injected reactant is readily consumed on a small area (Fig. 2a3). In that case, a medium injection rate Q increases A because it helps the spreading of the CO_3^{2-} solution. However, A is smaller for the largest Q because the flow is then strong enough to displace most particles towards the periphery (see Fig. 2b3,c3).

For large concentrations of both reactants (Fig. 5d), a similar trend to the one for I_{tot} is observed (Fig. 4f): beyond a critical Q, the area covered by the precipitate sharply drops and its spatial distribution is strongly localized producing hollow patterns (Fig. 2b5,c5).

We conclude from Fig. 5 that the largest area covered by the precipitate is reached at low injection rate Q if the reactants have similar concentrations (γ is not too large) (Fig. 5a and b). In contrast, when $\gamma = 18$ (Fig. 5c), the injected reactant is consumed by the displaced one over a smaller area leading to a lower A at a low flow rate.

5.2.2 Area A_p Enclosed by the Pattern.

In a non-reactive case, the area covered by the injected liquid increases linearly with the injected volume V if the thickness of the fluid layer is constant. In our system, with a gap width of 0.5 mm and an injection of a total of 2.5 mL of solution, one could expect a flooded area $A_{flood} = 50$ cm^2 if the parabolic profile of the injected liquid is neglected or $A_{flood} = 75$ cm^2 if it is taken into account. Figure 6 shows that, in most cases, the area A_p enclosed by the pattern indeed grows linearly with the injected volume and reaches a final value compatible with the one expected for non-reactive fluids.

There is however one noticeable exception at low injection rate Q when a diluted CO_3^{2-} solution is injected into a concentrated Ca^{2+} solution. As shown in Fig. 6b, A_p decreases indeed at low Q when the stoichiometric excess of the displaced solution increases. In addition, beyond some threshold of the initial concentration ratio γ, the growth of A_p is no longer linear and saturates once a given amount of reactant has been injected. At $\gamma = 18$, the large stoichiometric excess of the displaced solution leads to a rapid consumption of the CO_3^{2-} ions over a small area. At low Q, the precipitate is therefore not significantly advected and accumulates near the inlet. The precipitate is then progressively surrounded by the supernatant liquid (not visible on the image) leading to a significant decrease of A_p (Fig. 6b and Fig. 2a3). At larger Q, the precipitate is advected by the flow and A_p increases again linearly with V (Fig. 6e).

5.2.3 Filling.

The spatial homogeneity of the precipitate spatial distribution is characterized by the filling $F = A/A_p \in [0,1]$, the evolution of which is shown in Fig. 7 as a function of the injected volume. We see that, if the concentration of at least one of the reactants is low, F reaches a constant value close to 1 at low Q. The pattern is thus homogeneously filled by some precipitate (Fig. 2a1-4). For larger flow rates, F decreases because either the particles are advected away from the inlet (*e.g.* Fig. 2b1,c1) or fingering emerges (Fig. 2b4,c4).

If both reactants are concentrated, hollow structures appear once Q is large enough (Fig. 2b5,c5) and, consequently, F sharply drops (Fig. 7d). A slow increase of F is recovered at $Q = 1.0$ mL/min due to the emergence of secondary diffusive structures growing on a much larger time scale since the reactants need then to diffuse through the precipitate walls to meet and react (Fig. 2a5). At the largest Q, the wall may be even more

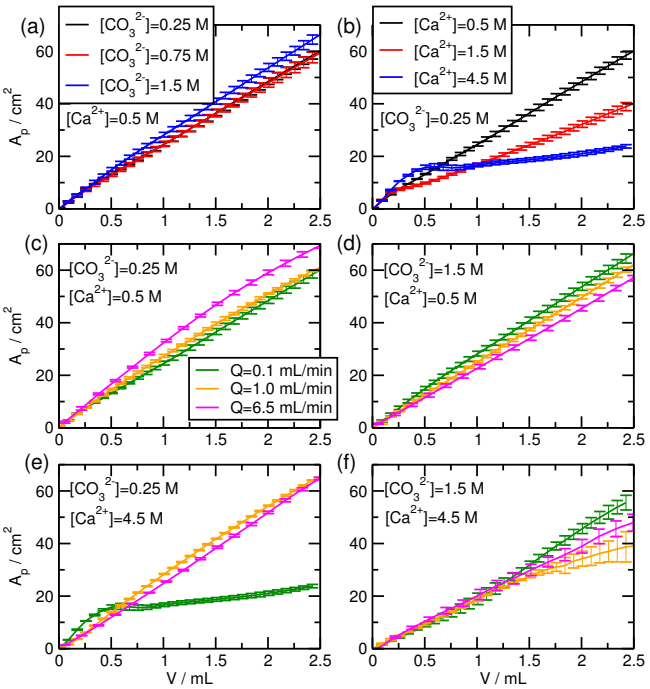

Fig. 6 Evolution of the area A_p, the zone inside the perimeter of the pattern, as a function of injected volume V of carbonate solution. $Q = 0.1$ mL/min for (a–b).

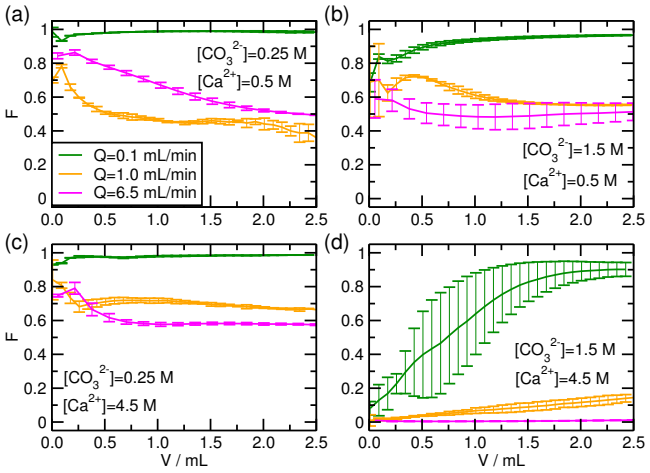

Fig. 7 Evolution of the filling of the pattern F as a function of injected volume V of carbonate solution at different flow rates and initial reactant concentrations.

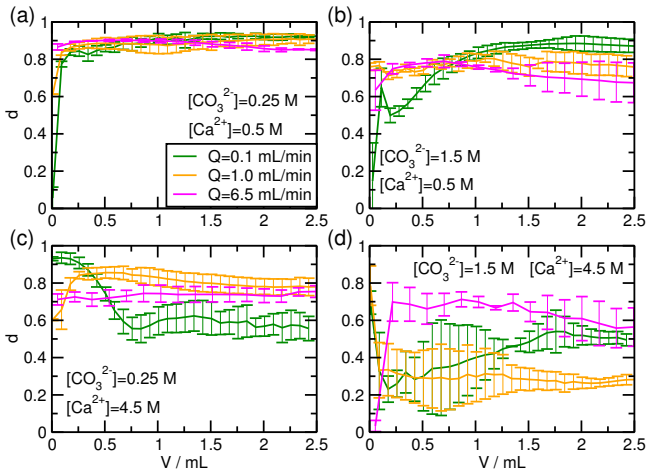

Fig. 8 Evolution of pattern density d as a function of injected volume V of carbonate solution at different flow rates and initial reactant concentrations.

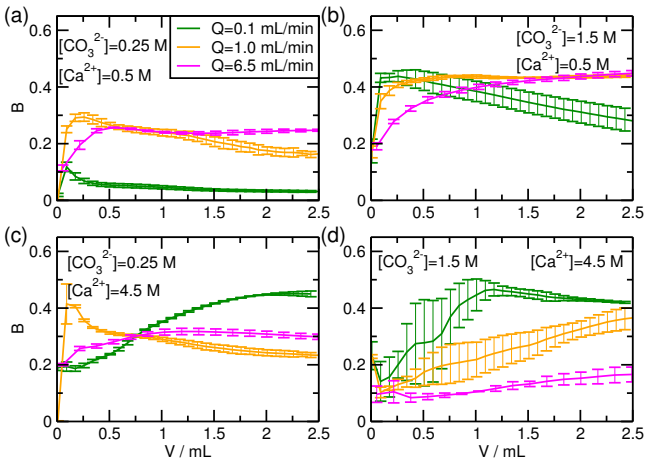

Fig. 9 Evolution of brightness B as a function of injected volume V of carbonate solution at different flow rates and initial reactant concentrations.

compact, hindering the growth of additional diffusive patterns in the hollow area during the timescale of the experiments, and hence F stays essentially at a constant low value.

In conclusion, Fig. 7 indicates that the most homogeneous spatial distributions of precipitate are obtained if at least one of the solutions is diluted and Q is low (see Table 1).

5.2.4 Pattern Density.

The deviation from a perfectly circular pattern is measured by the pattern density $d = A_p/(\pi R_{max}^2) \in [0,1]$, where R_{max} is the largest distance between the injection point and the pattern perimeter[17,30]. d measures indeed the homogeneity of the precipitate spatial distribution along the azimuthal direction (along circles of given radii). Patterns characterized by a low value of d tend to grow in some arbitrary preferred directions while, when d is close to one, any angular sector of the reactor, with a given angle, contains a similar amount of precipitate.

When the concentration of both reactants is low, the pattern is essentially circular with d close to 1 (see Fig. 8a and first column of Fig. 2). As seen in Fig. 4c, the precipitate production is enhanced in this regime of concentrations when Q increases. This affects the mobility ratio and produces moderate fingering[15] seen on the border of the patterns (Fig. 2a1,b1,c1).

Increasing the concentration of one reactant produces more precipitate (Fig. 4d,e) which leads to a larger deformation of the interface, *i.e.* to a decrease of d (Fig. 8b,c). When both solutions are concentrated (large SI_0 value), the precipitate forms solid walls which affects significantly the flow and strongly destabilize the interface leading to a low value of d (see the last column of Fig. 2, Fig. 8d, and the Movies of the experiments). In this case, the coupling between the formation of cohesive solid barriers and hydrodynamics makes the prediction of the precise location of the precipitate impossible.

These results show thus that the most homogeneous spatial spreading is reached if both the reactant concentrations and the injection flow rate Q are low (see Table 1). In this case, the thin precipitate layer does not impact significantly the hydrodynamics.

5.3 Brightness

The amount of precipitate per unit area it covers is proportional to the brightness $B = I_{tot}/A$, the evolution of which during injection is shown in Fig. 9. It is expected that a compact precipitate layer is produced if the concentrations and flow rate are large. Indeed, Fig. 9a and 9b show that raising Q leads to a larger value of B. When both concentrations are low (Fig. 9a), this increase of B with Q is due to the production of a larger amount of precipitate (Fig. 4c) over a smaller area (Fig. 5a). For larger concentrations of CO_3^{2-} (Fig. 9b), a larger flow rate induces the emergence of fingers where the precipitate accumulates (Fig. 2b4,c4). The increase of the brightness B is then mainly due to the decrease of the spatial distribution of the precipitate A, since I_{tot} is similar for all Q (Fig. 4d). However, when the concentration of the displaced solution is large, increasing Q has a negative impact on the brightness which decreases (Fig. 9c and 9d). The brightness can however still be large in these cases provided Q is low.

We conclude that the larger values of the brightness B are obtained at low flow rates if the displaced reactant is concentrated (Fig. 2a3 and 5) and at larger flow rates when a concentrated solution is injected into a diluted one (see Fig. 2b4,c4 and Table 1).

5.4 Production Efficiency

One way to quantify precipitation efficiency is to check how much precipitate can be produced per amount of reactant injected. This can be quantified by the production efficiency $P = I_{tot}/c_{0,CO_3^{2-}}$. Increasing P might be relevant for geological carbon dioxide sequestration for instance where the largest amount of mineralization is expected per amount of CO_2 injected. In this context, comparing Fig. 10a,b to Fig. 4a,b shows that like for I_{tot}, P evolves such that the larger the concentration of one reactant, the larger P and increasing the stoichiometric excess of the displaced solution (*i.e.* increasing Ca^{2+}) increases efficiency.

Increasing the flow rate to $Q = 6.5$ mL/min, while one reactant remains diluted and the concentration of the other one is increased, leads to different trends as depicted in Fig. 10c,d. At the lowest CO_3^{2-} concentration, P reaches a large value because

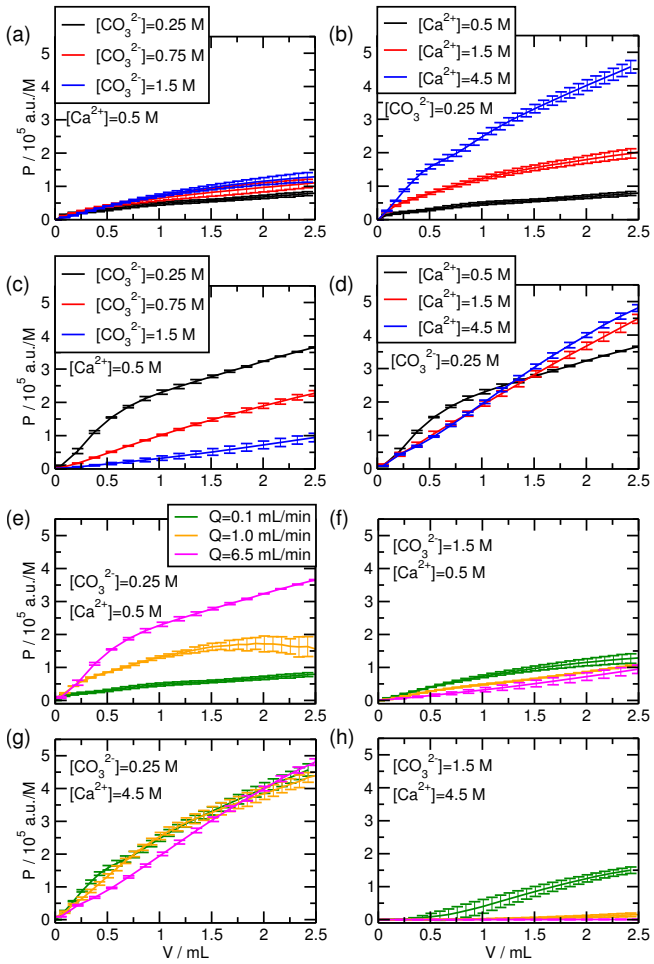

Fig. 10 Evolution of production efficiency P a function of injected volume V of carbonate solution. $Q = 0.1$ mL/min for (a–b) and $Q = 6.5$ mL/min for (c–d).

a larger Q ensures a better mixing. P decreases with increasing CO_3^{2-} concentration because the injected solution is in stoichiometric excess and cannot be consumed efficiently (Fig. 10c). For the opposite case, when the concentration of Ca^{2+} is increased while CO_3^{2-} is kept at a constant low value (Fig. 10d), P increases only slightly with the Ca^{2+} concentration. This shows that a large flow rate Q ensures the consumption of the injected reactant, such that increasing the excess of Ca^{2+} is then not necessary to increase P. In addition, precipitation is much more enhanced by increasing Q if the reactant concentrations are low and close to the stoichiometric ratio (compare Fig. 10a,c and 10b,d).

The evolution of P is shown in Fig. 10(e–h) for a given couple of reactant concentrations when Q varies. We see that a large P is reached if the CO_3^{2-} concentration is low and either Q or the concentration of the displaced reactant is large (Fig. 10e,g). When the concentration of CO_3^{2-} is large, P is always significantly smaller for all Q (Fig. 10f and 10h). In addition, when both concentrations are large, P even decreases when Q is increased (Fig. 10h).

Thus we conclude that a large precipitation efficiency P can be achieved either when both concentrations are low and Q is large or when the initial concentration ratio γ is large for all investigated Q (see Table 1).

Table 1 Optimal range of experimental conditions to obtain large values of I_{tot}, F, d, B, and P.

	Experimental conditions		
	$[Ca^{2+}]$	$[CO_3^{2-}]$	Q (mL/min)
I_{tot}	low	large	low
	large	large	low
F	low	low	low
	low	large	low
	large	low	low
d	low	low	low
B	low	large	medium and large
	large	low	low
	large	large	low
P	low	low	large
	large	low	any Q

6 Discussion

The efficiency of a precipitation reaction carried out in a confined geometry can be evaluated from various different point of views. In Sec. 5, five different quantitative measures describing the evolution of the precipitate patterns have been computed. They allow to discuss the efficiency of precipitation depending on whether the precipitation pattern

1. contains a large amount of precipitate (large I_{tot});
2. is homogeneously filled by particles, with few holes within the pattern periphery (large F value);
3. grows radially and spreads uniformly around the injection point (large d value);
4. accumulates on the smallest possible area, forming thick layers (large B value);
5. is such that the largest amount of injected reactant is effectively transformed into the solid precipitate (large P).

It can be supposed that, in most cases, the efficiency of transforming the reactants into a homogeneously distributed large amount of solid product corresponds to achieving large values of all the five quantities. It has however been shown in Sec. 5 that these different quantities reach their maximum in different optimal experimental condition ranges. A summary is presented in Table 1.

We see that using low concentrations and injecting at a low flow rate Q are the optimum conditions if a spatially homogeneous distribution of the precipitate is targeted since both the filling F and the pattern density d are then large. The reactant concentrations may however be increased if one needs to enhance the amount of precipitate produced (large I_{tot}) provided Q remains small. These experimental conditions also yield a compact precipitate layer (large B). In contrast, injecting at a larger flow rate Q is preferable if one wants to efficiently mineralize the injected reactant (large P), especially when the stoichiometric ratio of the reactants cannot be easily varied (*e.g.* the chemical composition of a geological formation).

Our results show thus that finding optimal experimental flow conditions such that both the spatial spreading and the amount of solid phase produced per injected reactant consumed are maximized is not obvious even in a simple confined geometry and for a simple reaction like studied here.

7 Conclusion

We have analyzed experimentally the properties of calcium carbonate precipitates obtained when injecting an aqueous solution of carbonate into a solution of calcium ions in a confined geometry at a controlled flow rate. Our objective was to quantify the experimental conditions optimizing the amount of solid phase produced as well as its spatial distribution. To do so, we have computed the total intensity I_{tot} of the white product precipitate, the filling F, the brightness B and the pattern density d of the solid structure produced as a function of the injected volume for various initial reactant concentrations and injection flow rate Q. We have moreover quantified the efficiency P giving an estimation of the quantity of solid phase produced per injected reactant consumed. We find that maximizing all these various quantities is not possible for one single set of experimental conditions. Indeed, very few solid strongly localized in space is obtained at high flow rates and large concentrations for instance while an optimized homogeneous spreading is rather reached for lower values of these quantities.

These conclusions show that out-of-equilibrium flow conditions can be efficiently used to optimize at will specific targets compared to precipitation under simple stirring for instance. For CO_2 mineralisation in sequestration techniques, our analysis also suggests that different operating conditions of injection of CO_2 into saline aquifers rich in minerals could be used depending whether a larger spatial distribution or a larger conversion of CO_2 into mineral carbonates is targeted. Of course, the simplicity of a Hele-Shaw cell and of the chemical solutions used here call for more elaborate studies on real 3D porous media[26] before reaching conclusive conclusions for sequestration techniques. Nevertheless, in view of the difficulties of *in-situ* analysis in real soils[25], we hope that the current approach will already shed some light into this complex problem.

Acknowledgments

The authors thank Prodex for financial support.

References

1 Sigel, A., H. Sigel and R. K. O. Sigel (Eds) (**2008**), Biomineralization: From Nature to Application. Metal Ions in Life Sciences **4**, Wiley-Blackwell, Hoboken, New Jersey.

2 Sancho-Tomás, M., S. Fermani, J. Gómez-Morales, G. Falini, and J. M. García-Ruiz (**2014**), Calcium Carbonate Bioprecipitation in Counter-diffusion Systems Using the Soluble Organic Matrix From Nacre and Sea-urchin Spine, *Eur. J. Min.*, *26*, 523–535.

3 Lagzi, I. (Ed) (**2010**), Precipitation Patterns in Reaction-Diffusion Systems, Research Signpost, Kerala, India

4 García-Ruiz, J.-M. (**2003**), Counter-diffusion Methods for Macromolecular Crystallization, *Methods in Enzymology*, *368*, 130-154.

5 Thouvenel-Romans, S., and O. Steinbock (**2003**), Oscillatory Growth of Silica Tubes in Chemical Gardens, *J. Am. Chem. Soc.*, *125(14)*, 4338–4341.

6 Baker, A., Á. Tóth, D. Horváth, J. Walkush, A. S. Ali, W. Morgan, Á. Kukovecz, J. J. Pantaleone, and J. Maselko (**2009**), Precipitation Pattern Formation in the Copper(II) Oxalate System with Gravity Flow and Axial Symmetry, *J. Phys. Chem.*, *113(29)*, 8243-8248.

7 Haudin, F., J. H. E. Cartwright, F. Brau, and A. De Wit (**2014**), Spiral Precipitation Patterns in Confined Chemical Gardens, *Proc. Nat. Acad. Sci. (USA)*, *111*, 17363–17367.

8 Richard, D. and T. Speck (**2015**), The Role of Shear in Crystallization Kinetics: From Suppression to Enhancement, *Scientific Reports*, *5:14610*, DOI: 10.1038/srep14610.

9 Bohner, B., G. Schuszter, O. Berkesi, D. Horváth, and Á. Tóth (**2014**), Self-organization of Calcium Oxalate by Flow-driven Precipitation, *Chem. Commun.*, *50*, 4289.

10 Bohner, B., B. Endrődi, D. Horváth, and Á. Tóth (**2016**), Flow-driven Pattern Formation in the Calcium-oxalate System, *J. Chem. Phys.*, *144*, 164504.

11 Bohner, B., G. Schuszter, D. Horváth, and Á. Tóth (**2015**), Morphology Control by Flow-driven Self-organizing Precipitation, *Chem. Phys. Lett.*, *631-632*, 114–117.

12 Haudin, F., J. H. E. Cartwright, and A. De Wit (**2015**), Direct and Reverse Chemical Garden Patterns Grown Upon Injection in Confined Geometries, *J. Phys. Chem. C*, *119*, 15067–15076.

13 Varghese, A. and S. Datta (**2012**), Directionally Asymmetric Self-assembly of Cadmium Sulfide Nanotubes Using Porous Alumina Nanoreactors: Need for Chemohydrodynamic Instability at the Nanoscale, *Phys. Rev. E*, *85*, 056104.

14 Tóth-Szeles, E., G. Schuszter, A. Tóth, Z. Kónya and D. Horváth (**2016**), Flow-driven Morphology Control in the Cobalt-oxalate System, *CrystEngComm*, *18*, 2057–2064.

15 Nagatsu, Y., Y. Ishii, Y. Tada, and A. De Wit (**2014**), Hydrodynamic Fingering Instability Induced by a Precipitation Reaction, *Phys. Rev. Lett*, *113*, 024502.

16 Haudin, F., V. Brasiliense, J. H. E. Cartwright, F. Brau, and A. De Wit (**2015**), Genericity of Confined Chemical Garden Patterns With Regard to Changes in the Reactants, *Phys. Chem. Chem. Phys.*, *17*, 12804–12811.

17 Haudin, F., and A. De Wit (**2015**), Patterns Due to an Interplay Between Viscous and Precipitation-driven Fingering, *Phys. Fluids*, *27*, 113101.

18 Schuszter, G., F. Brau and A. De Wit (**2016**), Calcium Carbonate Mineralization in a Confined Geometry, *Environ. Sci. Technol. Lett.*, *3(4)*, 156–159.

19 Barge, L. M., S. S. S. Cardoso, J. H. E. Cartwright, G. J. T. Cooper, L. Cronin, A. De Wit, I. J. Doloboff, B. Escribano, R. E. Goldstein, F. Haudin, D. E. H. Jones, A. L. Mackay, J. Maselko, J. J. Pagano, J. Pantaleone, M. J. Russell, C. I. Sainz-Díaz, O. Steinbock, D. A. Stone, Y. Tanimoto, and N. L. Thomas (**2015**), From Chemical Gardens to Chemobrionics, *Chem. Rev.*, *115(16)*, 8652–8703.

20 Pagano, J. J., T. Bánsági Jr., and O. Steinbock (**2008**), Bubble-templated and Flow-controlled Synthesis of Macroscopic Silica Tubes Supporting Zinc Oxide Nanostructures, *Angew. Chem. Int. Ed.*, *51*, 12754–12758.

21 Cartwright, J. H., B. Escribano, C. I. Sainz-Díaz, and L. S. Stodieck (**2011**), Chemical-garden Formation, Morphology, and Composition. II. Chemical Garden in Microgavity, *Langmuir*, *27(7)*, 3294-3300.

22 Batista, B. C. and O. Steinbock (**2015**), Growing Inorganic Membranes in Microfluidic Devices: Chemical Gardens Reduced to Linear Walls, *J. Phys. Chem. C*, *119(48)*, 27045-27052.

23 Haudin, F., L. A. Riolfo, B. Knaepen, G. M. Homsy, and A. De Wit (**2014**), Experimental Study of a Buoyancy-driven Instability of a Miscible Horizontal Displacement in a Hele-Shaw Cell, *Phys. Fluids*, *26*, 044102.

24 Shukla, P. and A. De Wit (**2016**), Fingering Dynamics Driven by a Precipitation Reaction: Nonlinear Simulations, *Phys. Rev. E*, *93*, 023103.

25 Matter, J. M., M. Stute, S. Ó. Snæbjörnsdottir, E. H. Oelkers, S. R. Gislason, E. S. Aradottir, B. Sigfusson, I. Gunnarsson, H. Sigurdardottir, E. Gunnlaugsson, G. Axelsson, H. A. Alfredsson, D. Wolff-Boenisch, K. Mesfin, D. F. de la Reguera Taya, J. Hall, K. Dideriksen, W. S. Broecker (**2016**) Rapid Carbon Mineralization for Permanent Disposal of Anthropogenic Carbon Dioxide Emissions, *Science*, *352(6291)*, 1312–1314.

26 Luquot, L. and Gouze, P. (**2009**) Experimental Determination of Porosity and Permeability Changes Induced by Injection of CO_2 into Carbonate Rocks, *Chem. Geo.*, *265*, 148–159.

27 White, A.R., and T. Ward (**2012**), CO_2 Sequestration in a Radial Hele-Shaw Cell via an Interfacial Chemical Reaction, *Chaos*, *22*, 037114.

28 Tartakovsky, A. M., G. Redden, P. C. Lichtner, T. D. Scheibe, and P. Meakin (**2008**), Mixing-induced Precipitation: Experimental Study and Multiscale Numerical Analysis, *Water Resources Research*, *44*, W06S04, doi:10.1029/2006WR005725.

29 Zhang, C., K. Dehoff, N. Hess, M. Oostrom, T. W. Wietsma, A. J. Valocchi, B. W. Fouke, J. C. Werth (**2010**), Pore-Scale Study of Transverse Mixing Induced $CaCO_3$ Precipitation and Permeability Reduction in a Model Subsurface Sedimentary System, *Environ. Sci. Technol.*, *44*, 7833–7838.

30 Chen, J.-D. (**1989**) Growth of Radial Viscous Fingers in a Hele-Shaw Cell, *J. Fluid Mech.*, *201*, 223–242.